Protein Conformational Gating of Enzymatic Activity in Xanthine Oxidoreductase

Hiroshi Ishikita,*,[†,‡] Bryan T. Eger,[§] Ken Okamoto,[∥] Takeshi Nishino,[∥,⊥,#] and Emil F. Pai[§,¶]

[†]Career-Path Promotion Unit for Young Life Scientists, Kyoto University, 202 Building E, Graduate School of Medicine, Yoshida-Konoe-cho, Sakyo-ku, Kyoto 606-8501, Japan

[‡]Japan Science and Technology Agency (JST), PRESTO, 4-1-8 Honcho Kawaguchi, Saitama 332-0012, Japan

[∥]Department of Biochemistry and Molecular Biology, Nippon Medical School, 1-1-5 Sendagi, Bunkyo-ku, Tokyo 113-8602, Japan

[§]Department of Biochemistry, University of Toronto, 1 King's College Circle, Toronto, ON, M5S 1A8, Canada

[¶]Departments of Medical Biophysics and Molecular Genetics, University of Toronto, 1 King's College Circle, Toronto, ON, M5S 1A8, Canada and The Campbell Family Cancer Research Institute/Ontario Cancer Institute, University Health Network, MaRS/TMDT, 101 College Street, Toronto, ON, M5G 1L7, Canada

[⊥]Department of Biochemistry, University of California, 1463 Boyce Hall, Riverside, California 92521-0122, United States

[#]Department of Applied Biological Chemistry, Graduate School of Agricultural and Life Sciences, University of Tokyo, 1-1-1 Yayoi, Bunkyo-Ku, Tokyo, 113-8657, Japan

S *Supporting Information*

ABSTRACT: In mammals, xanthine oxidoreductase can exist as xanthine dehydrogenase (XDH) and xanthine oxidase (XO). The two enzymes possess common redox active cofactors, which form an electron transfer (ET) pathway terminated by a flavin cofactor. In spite of identical protein primary structures, the redox potential difference between XDH and XO for the flavin semiquinone/hydroquinone pair ($E_{sq/hq}$) is ~170 mV, a striking difference. The former greatly prefers NAD^+ as ultimate substrate for ET from the iron–sulfur cluster FeS-II via flavin while the latter only accepts dioxygen. In XDH

(without NAD^+), however, the redox potential of the electron donor FeS-II is 180 mV higher than that for the acceptor flavin, yielding an energetically uphill ET. On the basis of new 1.65, 2.3, 1.9, and 2.2 Å resolution crystal structures for XDH, XO, the NAD^+- and NADH-complexed XDH, $E_{sq/hq}$ were calculated to better understand how the enzyme activates an ET from FeS-II to flavin. The majority of the $E_{sq/hq}$ difference between XDH and XO originates from a conformational change in the loop at positions 423−433 near the flavin binding site, causing the differences in stability of the semiquinone state. There was no large conformational change observed in response to NAD^+ binding at XDH. Instead, the positive charge of the NAD^+ ring, deprotonation of Asp429, and capping of the bulk surface of the flavin by the NAD^+ molecule all contribute to altering $E_{sq/hq}$ upon NAD^+ binding to XDH.
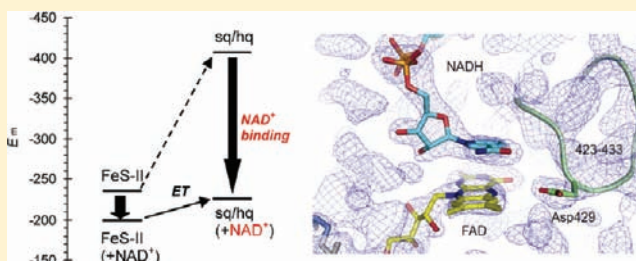
Xanthine oxidoreductase catalyzes the hydroxylation of either hypoxanthine to xanthine or xanthine to uric acid. In mammals, the enzyme is synthesized as xanthine dehydrogenase (XDH), its most prevalent form. It can, however, be converted to its xanthine oxidase (XO) form, either reversibly by disulfide formation or irreversibly by proteolytic cleavage, a transformation that plays important roles in physiological and pathological processes. In both forms, the enzyme is a homodimer of 290 kD and contains a variety of redox active cofactors, which line up to form the ET pathway. Electrons enter at the molybdopterin center and proceed via two Fe_2S_2 type iron–sulfur clusters, FeS-I and FeS-II, to the flavin adenine dinucleotide (FAD) cofactor (Figure 1).

The most pronounced difference between XDH and XO is their terminal electron acceptor. XDH strongly prefers NAD^+ over molecular oxygen, O_2, while XO cannot bind NAD^+ and therefore can only use O_2.[1,2] Indeed, of all the redox active cofactors in the ET pathway, flavin is the only one that changes its redox properties significantly during the conversion from XDH to XO; in particular, the redox potential for the flavin semiquinone (sq)/ hydroquinone (hq) pair ($E_{sq/hq}$) is notably different. The $E_{sq/hq}$ values are −410 mV for XDH (at pH 7.5[3]) and −234 mV for XO (at pH 7.7[4]), thus resulting in an $E_{sq/hq}$ upshift of ~170 mV. The resulting ~170 mV difference implies that the flavin electrostatic environment is considerably different in the two enzymes. On the other hand, the apparently different protein environments of the two enzymes yield quite a similar value with regards to the redox potential for the oxidized flavin (ox)/semiquinone pair ($E_{ox/sq}$): −270 mV for XDH (at pH 7.5[3])
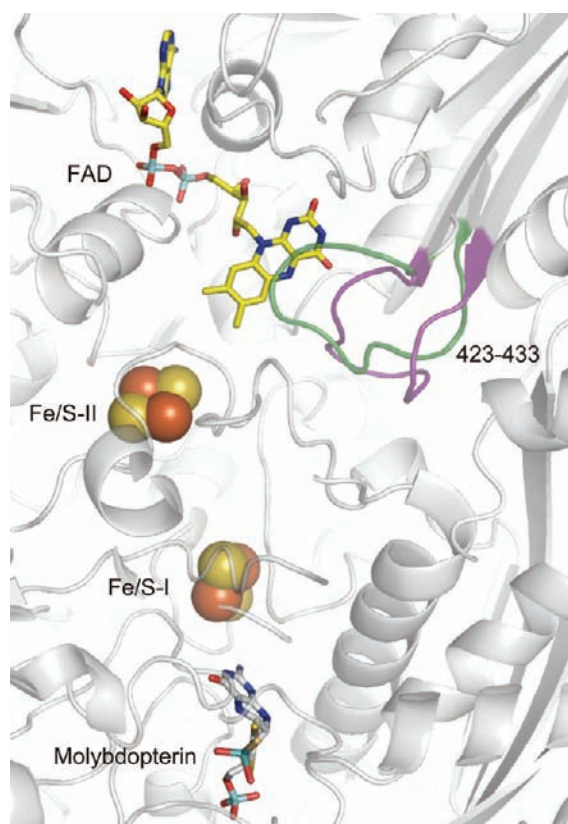
Figure 1. Cofactor arrangements in xanthine oxidoreductase. The 423−433 loops in the neighborhood of the flavin binding sites are depicted as pink (XDH) and green (XO) threads, respectively.

and −332 mV for XO (at pH 7.7[4]). Crystal structures of XDH and XO revealed that the two proteins differ in particular in the orientation of a loop region (Gln423-Lys433) near the flavin binding moiety.[5] However, no additional highly refined information to the flavin energetics in the protein environment is available yet.

In XDH, the reduction of NAD^{+} occurs through the hq form of the flavin in a two electron (hydride) transfer process. To facilitate the formation of NADH, it is necessary to favor the hq form over the sq form. To achieve this goal, efficient ET from FeS-II to the flavin is also required. However, the $E_{sq/hq}$ value of −410 mV is much lower than the E_m value of −235 mV for the electron donor FeS-II,[3] yielding an energetically uphill ET (+175 meV). Note that $\Delta G_{ET} = -nF\Delta E \approx -[E_m(\text{acceptor}) - E_m(\text{donor})]$ [meV] where $\Delta G_{ET} < 0$ or > 0 describe an energetically downhill or uphill ET process, respectively (e.g., see ref 6).

One way to achieve this goal could be that NAD^{+} binding to XDH changes the energetics of ET (reviewed in ref 7), for example, by triggering a conformational change similar to the one observed in the 423−433 loop near the flavin binding site upon conversion from XDH to XO.[5] Such a change might upshift $E_{sq/hq}$ from −410 mV to −230 mV (i.e., 180 mV upshift) and make ET from FeS-II (E_m = −235 mV[3]) to the flavin isoenergetic. The lack of crystal structures of nicotinamide dinucleotide complexes of XDH or XO, however, has left this question unanswered.

We now report the 1.65, 2.3, 1.9, and 2.2 Å resolution crystal structures of the bovine XDH, XO, and NAD^{+} and NADH complexes of XDH. One of the aims of the present study was to better understand the aspects of flavin-protein interaction,

namely the factors that increase the $E_{sq/hq}$ difference up to ~170 mV as well as those that eliminate the $E_{ox/sq}$ difference in XDH and XO. The present crystal structures also provide the structural implication how NAD^{+} can bind close to FAD in a π-stacking geometry, which enables NAD^{+} to serve as an electron acceptor to FAD. Another major aim of the present study is, thus, to elucidate how the protein achieves an energetically uphill ET[7,8] (based on the E_m values for FeS-II and flavin in ligand-free XDH[3]). To specifically focus on this point, although we had been able before to investigate the pH-dependence of the E_m sufficiently well (for instance, see refs 9 and 10), the present study describes the contributions of protein residues and cofactors to $E_{sq/hq}$ at pH 7.8, the pH value at which most biochemical measurements were performed (reviewed in ref 11). The computational conditions and procedures used in our previous studies on flavin-containing proteins (e.g., flavodoxin[12,13] and the BLUF domain[14]) were also applied in the present study.

EXPERIMENTAL PROCEDURES

Crystallography. Bovine XDH and XO were purified from milk and crystallized as published.[15] The XDH−NADH complex was prepared by soaking native XDH crystals for 1.5 h at room temperature in mother liquor containing 33 mM NADH. The XDH−NAD^{+} complex was generated by crystallizing XDH in the presence of 667 μM NAD^{+}. Data for the XDH crystal were collected in two passes, a high- and a low-resolution pass, at beamline BL40B2 of the Spring-8 synchrotron, and in single passes for XO and the XDH−NADH complex on beamlines BL17A and NW12A of the Photon Factory (Tsukuba), and for the XDH-NAD^{+} complex on beamline 14-BM-C at the Advanced Photon Source. Data were reduced using the program package HKL2000.[16] The starting atomic model of XDH for refinement by CNS[17] was the one deposited in the PDB under access code 1FO4.[5] The same structure was used as search model to determine the structures of the XDH complexes using the molecular replacement program EPMR.[18] For the structure of the XO dimer the model 1FIQ and the program MOLREP[19] were used. Refinements were performed employing CCP4, version 6.1.[20] Model building was done with the help of the programs O[21] and Coot.[22] Atomic coordinates and structure factors have been deposited in the RCSB PDB under the access codes 3UNC for XDH, 3AX9 for XO, 3UNA for NAD^{+}-bound XDH, and 3UNI for NADH-bounded XDH.

Atomic Coordinates and charges. As basis for the computations, the high-resolution crystal structure of ligand-free bovine milk XDH (PDB) code 3UNC) and the structure of ligand-free XO (PDB code 3AX9) as well as the NADH- (PDB code 3UNA) and NAD^{+}-complexed XDH (PDB code 3UNI) were used. The NADH-complexed XDH structure had to serve as a geometry template to model the NAD^{+} complex because when NAD^{+} is bound to oxidized XDH only the adenine half of the molecule is visible in the electron density map with the nicotinamide half highly mobile and invisible. Although the model of XDH complexed to NAD^{+} is missing the atoms of the nicotinamide, its ribose and the adjacent phosphate group, the two crystal structures essentially did not differ in the position/orientation of the flavin ring, the remaining parts of the NAD^{+}/NADH molecules, and the loop 423−433 (backbone as well as side chains). Using the crystal structure of XDH complexed to NADH for calculations of the XDH structure complexed to NAD^{+} is, therefore, the best possible starting point and in part justified by structural evidence. Since under physiological conditions, NAD^{+} will not bind properly to XDH as long as the flavin is oxidized, the present procedure should be used only for calculations of the flavin sq/hq form.

The positions of the H atoms were energetically optimized with CHARMM[23] by using the CHARMM22 force field. During this procedure, the positions of all non-H atoms were fixed, and the standard charge states of all the titratable groups were maintained, that is, basic and acidic groups were considered to be protonated and deprotonated, respectively. The two iron−sulfur Fe_2S_2 centers, FeS-I and FeS-II, were in the oxidized state and the flavin isoalloxazine ring

1000

dx.doi.org/10.1021/ja207173p | *J. Am. Chem. Soc.* 2012, 134, 999−1009

was in the neutral charge state. All the other atoms whose coordinates were available in the crystal structure were not geometrically optimized.

Atomic partial charges of the amino acids were adopted from the all-atom CHARMM22[23] parameter set. The charges of the Fe_2S_2 iron−sulfur clusters were taken from ref 24 and the same as in our previous studies.[25] The charges of the isoalloxazine ring of flavin were taken from our previous studies of flavin mononucleotide (FMN, FMN•−, and FMNH•: that correspond to FAD, FAD•−, and FADH•, respectively) in flavodoxins[12,13] and the BLUF domains.[14] The charges of the adenosine part of flavin were adopted from the all-atom CHARMM22 parameter set. The pyrophospate parts of FAD and NAD+/NADH were treated as comprised of two independent phosphate titratable sites (Table S1 in the Supporting Information). For each titratable site, we prepared for both protonated and deprotonated states of the charges by referring to the diphosphate charge of the ATP and ADP entries in CHARMM. The charges of the molybdopterin center and nicotinamide NAD+/NADH were determined from the electronic wave functions by fitting the resulting electrostatic potential in the neighborhood of these molecules by using the restrained electrostatic potential (RESP) procedure.[26] The electronic wave functions were calculated with the density functional (DFT) module in Gaussian03[27] by using the B3LYP functional with the LANL2DZ and 6-31+G** basis sets for Mo and other atoms, respectively (Tables S2 and S3 in the Supporting Information). The charges of the titratable phosphate group of the molybdopterin center were taken from our previous studies.[12−14] All presented results were obtained in the presence of the Mo(VI) state.

Protonation Pattern, Redox Potential, and pK_a. The present computation is based on the electrostatic continuum model created by solving the linear Poisson−Boltzmann (LPB) equation with the MEAD program.[28] To facilitate a direct comparison with previous computational results, we used identical conditions and parameters such as atomic partial charges and dielectric constants. To obtain the absolute redox midpoint potential values of the protein, we calculated the electrostatic energy difference between the two redox states in a reference model system using a known experimental E_m value. The difference in the E_m value of the protein relative to the reference system was added to the known E_m value (see below). All other titratable sites, including the flavin pyrophosphate group, were fully equilibrated to the flavin redox state during the titration. The ensemble of the protonation patterns was sampled by the Monte Carlo (MC) method with Karlsberg[29] (Rabenstein, B. *Karlsberg online manual*, http://agknapp.chemie.fu-berlin.de/karlsberg/ (1999)). The dielectric constants were set to $\varepsilon_p = 4$ inside the protein and $\varepsilon_w = 80$ for water. All computations were performed at 300 K, pH 7.8, and an ionic strength of 100 mM. The LPB equation was solved using a three-step grid-focusing procedure at resolutions of 2.5, 1.0, and 0.3 Å. The MC sampling yielded the probabilities $[A_{ox}]$ and $[A_{red}]$ of the two redox states of molecule A. E_m was evaluated using the Nernst equation. A bias potential was applied to obtain an equal amount of both redox states ($[A_{ox}] = [A_{red}]$), thereby yielding the redox midpoint potential E_m as the resulting bias potential. From this analogy, using the Henderson−Hasselbalch equation, the pK_a can be calculated as the pH at which the concentrations of the protonated and deprotonated residue species are equal (Henderson−Hasselbalch pK_a). For convenience, the computed E_m value is given with mV accuracy, without implying that the last digit is significant. In general, an E_m value of approximately 10 mV is a sufficiently reproducible range for the computational method used (e.g.[12−14,25,30]).

pK_a Value in the Reference Model System. FAD•− forms FADH• upon protonation at the N5 nitrogen in FAD. The value of 8.6[31] was taken as the pK_a(N5) value in the reference model system of FADH•/FAD•− equilibrium in aqueous solution. Experimentally measured pK_a values of the pyrophosphate part of FAD and NAD+/NADH are not known. The values should be close to the values for pyrophosphoric acid; 0.85, 1.49, 5.77, and 8.22 (Stryer, L., (1988) Biochemistry third edition, Appendix C). In the present study, the pyrophospate parts of FAD and NAD+/NADH were treated as comprised of two independent phosphate titratable sites (Table S1 in the Supporting Information). Accordingly, we tentatively used the pK_a

value of 1.5 for each phosphate titratable site as the value in the reference system (i.e., isolated aqueous solution), derived from the pK_a values of dimethyl- or dipropyl- phosphate.[32] In XO, the two phosphate titratable sites of FAD were deprotonated. In XDH, however, phosphate titratable sites of the FAD diphosphate region distal and proximal to the flavin ring (distal and proximal phosphates) were deprotonated and protonated, respectively. In the NAD+ diphospate region, one titratable site was deprotonated but the other largely protonated (by ~0.7 H+). The influence of the phosphate on $E_{sq/hq}$ in XDH and XO will be discussed in detail later. The value of 6.4[33] was considered as the pK_a value in the molybdopterin-phosphate group ($-H_2PO_3^-/-HPO_3^{2-}$).

Calculation of $E_{sq/hq}$ as E_m(FADH•/FADH−). The $E_{sq/hq}$ value of −172 mV for free flavin measured by Draper and Ingraham with potentiometry[31] was used as the reference model system. Since protonation/deprotonation at the N1 nitrogen of the flavin isoalloxazine ring occurs at pK_a = 6.7 in aqueous solution[31]), the N1 site was considered to be deprotonated under the condition investigated. Note that the redox process for quinone is the simple addition of an electron in the pH-independent region where the protonation process can be ignored.[34]

Calculation of $E_{ox/sq}$ as E_m(FAD/FADH•). The reaction involving FAD yielding FADH• that has an E_m(FAD/FADH•) is the process in which one-electron reduction of FAD to FAD•− is coupled with protonation at the N5 nitrogen atom. Contribution of protonation/deprotonation at the N5 atom to $E_{ox/sq}$ cannot be ignored since pK_a(N5) = 8.6.[31] Indeed, $E_{ox/sq}$ shows a pH dependence of −60 mV/pH unit around pH 7.5.[35] Therefore, one has to consider the energetics of both the "one-electron redox process" and the "one-proton protonation process" to accurately estimate the net energetics.

The potential of proton-coupled one-electron reduction can be written as follows:

$$E_m(FAD/FADH^\bullet) = E_m(FAD/FAD^{\bullet-})$$
$$+ RT/F\ln 10\log(1 + 10^{-pH}/10^{-pKa(N5)}) \quad (1)$$

where R is the gas constant, T is the temperature, and F is the Faraday constant (see ref 36).

To use eq 1, the E_m(FAD/FAD•−) value in aqueous solution as the reference model system is needed. By using E_m(FAD/FADH•) = −238 mV at pH 7 and pK_a(N5) = 8.6[31] (summarized in ref 37), E_m(FAD/FAD•−) = −333 mV was obtained from eq 1. This value was used as the reference model system of E_m(FAD/FAD•−) in aqueous solution.

Protein Dielectric Volume and Treatment of Water. The dielectric volume of a protein complex is the spatial area and shape of molecular components of the protein and includes the polypeptide backbone, side chains, and cofactors. As a general and uniform strategy, all of the crystallized water molecules were removed for our computations due to the lack of experimental information regarding the H atom positions. Cavities that formed after removal of the crystallized water molecules were uniformly filled with a dielectric solvent ($\varepsilon_w = 80$). By doing such, the effect of the removed water molecules was considered implicitly and a high value for the dielectric constant was assigned to these cavities (for evaluation of the dielectric constant in the protein, see discussion in the Supporting Information).

■ RESULTS AND DISCUSSION

1. XDH and XO. *High-resolution Crystal Structure of XDH.* The 1.65 Å resolution structure confirms the overall fold of the dimeric protein, the location of the cofactors and the mobile stretches of the polypeptide chain.[5] The greatly improved quality of the new electron density map, however, allowed the placement of a total of 1966 water molecules, 24 glycerol molecules and 2 Ca^{2+} ions (Table 1). Also, multiple conformations were identified for side chains and their respective occupancies were assigned.

$E_{sq/hq}$ in XDH and XO. The calculated $E_{sq/hq}$ values were −407 mV for XDH and −268 mV for XO (Table 2), resulting

Table 1. Data Collection and Refinement Statistics of Bovine XDH/XO Crystal Structures

	XDH	XO	XDH+NAD$^+$	XDH+NADH
Space group	C2	P2$_1$	C2	P2$_1$
Unit cell axes (Å)	a = 167.6	a = 133.2	a = 166.0	a = 100.0
	b = 124.4	b = 73.0	b = 123.2	b = 146.7
	c = 148.2	c = 142.3	c = 147.6	b = 107.0
Unit cell angle β (°)	91.1	98.8	91.0	106.0
Resolution limits (Å)	20–1.65	38.1–2.30	20.0–1.90	20.0–2.20
I/σ I (Last Shell)	25.5 (2.9)^a	9.5 (3.7)	23.6 (3.8)	14.8 (3.6)
Linear R-factor (%)	5.3 (45.4)	11.7 (34.7)	6.4 (38.0)	9.0 (37.7)
Completeness All Data (%)	99.9 (99.9)	99.3 (96.1)	99.8 (98.9)	99.9 (99.9)
Overall redundancy	4.27	3.40	5.33	3.08
R-cryst (%)	17.7	21.8	18.1	19.8
R-free (%)	19.6	27.9	21.4	24.0
Number of atoms (All)	22322	19797	21842	21497
Number of water molecules	1966	651	1509	1140
Number of glycerol molecules	24	5	13	10
Number of Ca^{2+} ions	2	2	2	2

^{a}Numbers in brackets refer to the highest resolution shell.

Table 2. Analysis of $E_{sq/hq}$ in mV

		XDH	XO	Difference^a	XDH+NAD$^+$	XDH+NADH
$E_{sq/hq}$	experimental	−410^b	−234^c	−176	n.d.	n.d.
	calculated	−407	−268	−139	−226	−346
	uncharged protein^d	−343	−347	4	−406	−400
	reference (water)^e	−172	−172	0	−172	−172
$E_{sq/hq}$ shift	Total	−235	−96	−139	−54	−174
(from water to protein)	$\Delta E_{sq/hq}$ (charge)^f	−64	79	−143	180	54
	$\Delta E_{sq/hq}$ (dielectric volume)^g	−171	−175	4	−234	−228

$^a E_m$(XDH) − E_m(XO). ^{b}At pH 7.5.[3] ^{c}At pH 7.7.[4] ^{d}Prepared by setting atomic charges of all atoms in the protein to zero. ^{e}See ref 31. ^{f}Influence of atomic charge of all atoms in the protein. ^{g}Influence of uncharged protein dielectric volume (i.e., the space covered by the merged van der Waals volumes of protein atoms).

in the significant $E_{sq/hq}$ difference of ∼140 mV. These values are close to the experimentally measured values of −410 mV for XDH[3] and −234 mV for XO.[4] During titration experiments to determine $E_{sq/hq}$, some titratable sites change their protonation states in response to the flavin redox state. Since, in XDH, the carboxyl O atom of Asp429 is 4.6 Å away from the flavin N5 atom, the protonation state of Asp429 is strongly coupled with the flavin redox state (Figure 3). In contrast, the corresponding titration curve of XO is considerably different from that of XDH. In response to changes in the flavin redox state, there were no residues that strongly coupled with regards to their protonation states. The absence of coupling of the Asp429 protonation state with the flavin redox state in XO is due to the fact that the O$_{Asp429}$−N5$_{FAD}$ distance in XO has increased to 11.9 Å (Figure 2).

Contribution of Protein Dielectric Volume to the $E_{sq/hq}$ Difference in XDH and XO. The protein dielectric volume (i.e., the space obtained by merging the volumes of the van der Waals spheres of all protein atoms) is a main part of what provides so-called "protein hydrophobicity" to the flavin: the protein dielectric volume prevents access of water molecules to the flavin, and thus decreases the availability of solvation energy. In particular, the loss of solvation energy[38] destabilizes the flavin reduced state significantly, leading to the decrease in the redox potential.

By comparing the $E_{sq/hq}$ value of the flavin in water (−172 mV) with the $E_{sq/hq}$ value of the "uncharged" protein (i.e., where all the atomic partial charges in the protein except the flavin part

(flavin = isoalloxazine ring and ribitol region) are set to zero, −343 mV for XDH and −347 mV for XO), the influence of protein dielectric volume on $E_{sq/hq}$ is calculated as −171 and −175 mV, respectively (Table 2). In the two enzymes, the protein dielectric volume destabilizes the flavin reduced state significantly.

The difference in the protein dielectric volume for the two enzymes is essentially zero, indicating that the influence of the protein dielectric volume is not a main factor that differentiates the $E_{sq/hq}$ values for XDH and XO (relative to the entire $E_{sq/hq}$ difference of ∼170 mV).

Influence of the Atomic Charge on the $E_{sq/hq}$ Difference for XDH and XO. From comparison between the calculated $E_{sq/hq}$ value for the protein and the calculated $E_{sq/hq}$ value for the "uncharged" protein, the influence of the protein atomic charge on $E_{sq/hq}$ can be obtained. In the present study, the $E_{sq/hq}$ values are shifted by −64 mV for XDH and 79 mV for XO due to the atomic partial charges on the entire protein (Table 2). The difference in the atomic charge contribution (143 mV) accounts for a majority of the $E_{sq/hq}$ difference (139 mV) for XDH and XO. The influence of atomic charge of the protein on $E_{sq/hq}$ is a sum of influences from each atom of the entire protein molecule. This enables us to clarify the influence of each residue/group on $E_{sq/hq}$.

A number of residues located in/near the loop of Gln423-Lys433 significantly influence the $E_{sq/hq}$ for both XDH and XO (Table 3a). For the two enzymes, Lys422 (160−260 mV), Arg426 (90−130 mV), and Lys433 (40−150 mV) are notable with regard to the $E_{sq/hq}$ upshift. Lys1228 (80−130 mV) and
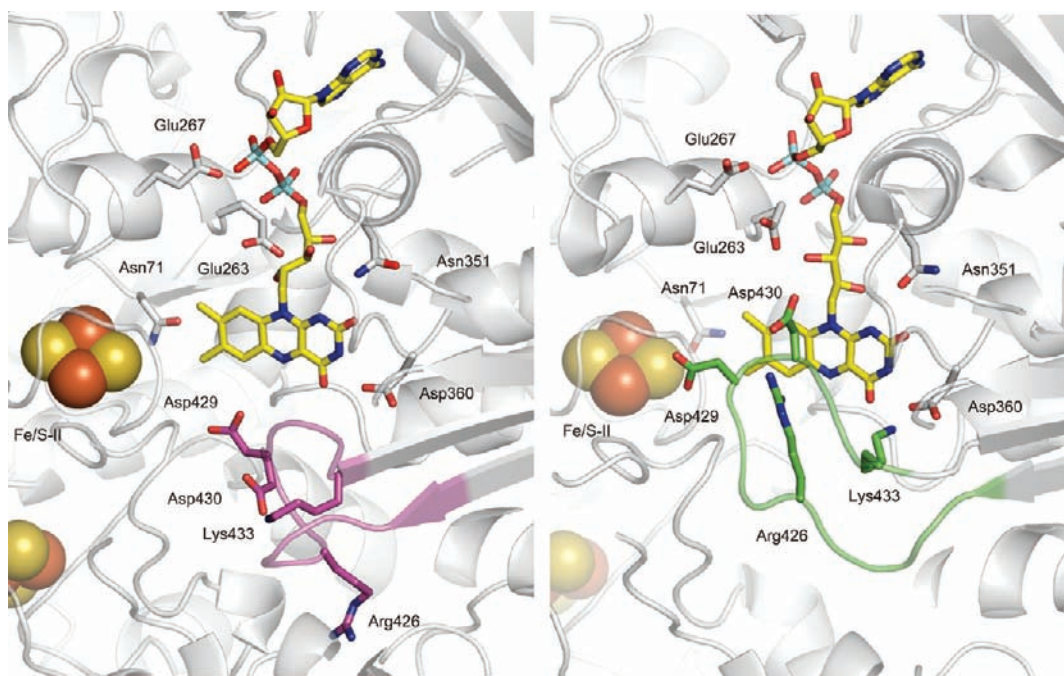
Figure 2. Structural overview of the location of the flavin ring of FAD and the iron−sulfur clusters (FeS-I and FeS-II) in XDH (left) and XO (right). The 423−433 loops in the neighborhood of the flavin binding sites are depicted as pink (XDH) and green (XO) threads, respectively.
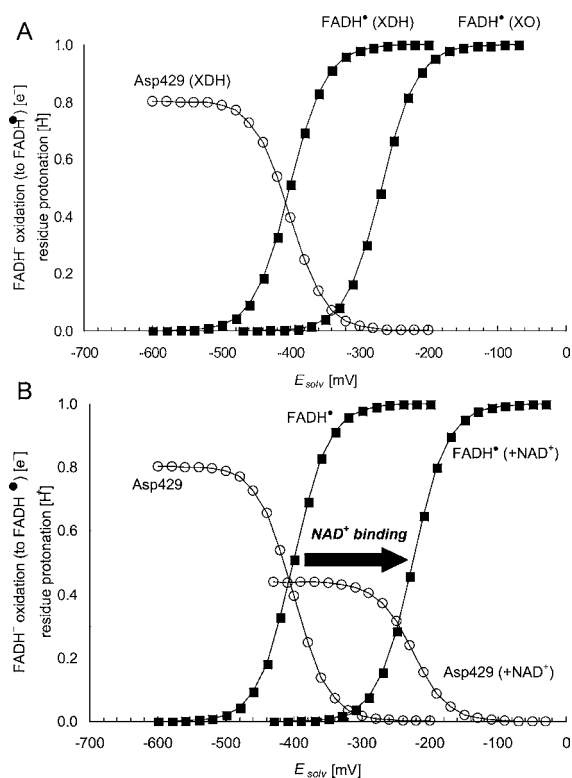

Figure 3. (a) Redox titration for the flavin $E_{sq/hq}$ value (■) versus solvent potential (E_{solv}) in XDH and XO. Associated changes in the protonation state of Asp429 as deprotonation state (i.e., 1.0 for fully deprotonated ionized state and 0.0 for fully protonated neutral state) are also shown (○). (b) Shift in the titration curves upon NAD$^+$ binding (solid black arrow). The NAD$^+$ redox state is fixed while titrating $E_{sq/hq}$. For definitions of protonation and redox probabilities, see ref 53.

Lys343 (70−90 mV) near the flavin binding site also increase the $E_{sq/hq}$ values in the two enzymes, although the two residues

do not belong to the loop. For the $E_{sq/hq}$ downshift, Asp360 (190−240 mV, 2.7 Å from the flavin N3 atom in XDH and 2.6 Å for XO, Figure 2) and a negatively charged iron−sulfur cluster, FeS-II (130−150 mV), have the largest impact.

We found that the 423−433 loop is important for the large influence on $E_{sq/hq}$ and the resulting $E_{sq/hq}$ difference between the two enzymes. Especially, Lys433, Asp429, Asp430, and Arg426 are key residues that differentiate the $E_{sq/hq}$ for XDH and XO significantly: each residue contributes to increasing the $E_{sq/hq}$ difference by 40−100 mV in XDH and XO. As a consequence, residues that are part of the stretch from position 422 to 433 are responsible for the $E_{sq/hq}$ difference of 137 mV for XDH and XO (Table 3b). Indeed, the protein conformations differ dramatically in this loop as revealed in the crystal structures[5] (Figure 2), confirming that redox potential is determined by the protein geometry alone.[12]

FeS and Mo. In general, iron sulfur clusters lower the redox potential of a redox active group. For instance, in Photosystem I, the three iron sulfur clusters F_X, F_A and F_B are located near the two quinones and responsible for downshifts of the quinone redox potentials: for F_X by 240−260 mV, for F_A by 30−50 mV, and for F_B by 10−20 mV (edge-to-edge distances to the quinones are ∼7, 20, and 30 Å, respectively).[25] In XDH and XO, the flavin ring is ∼7 Å from FeS-II as is the case with F_X and the quinones in Photosystem I. Indeed, the influence of FeS-II's atomic charge on $E_{sq/hq}$ is significant for XDH and XO. FeS-II and FeS-I are responsible for quite large $E_{sq/hq}$ downshifts of 130−150 mV and 40 mV, respectively (Table 3).

Since the Mo center is ∼30 Å away from the FAD binding site, its influence (including that of its phosphate region) on $E_{sq/hq}$ is quite marginal, downshifting $E_{sq/hq}$ by only 13 mV (5 mV due to the phosphate region and 8 mV due to the remaining parts) in both XDH and XO. In agreement with the present computational result, experimental measurements clearly demonstrate that the molybdopterin part does not have a significant influence on the

Table 3. (a) Protein Components Differentiating the $E_{sq/hq}$ Value for XDH/XO in mV and (b) Influence of the Atomic Charges of Residues in the 423−433 Loop (including Lys422) on the $E_{sq/hq}$ Value for XDH/XO in mV[a]

a	$E_{sq/hq}$(XDH)	$E_{sq/hq}$(XO)	difference[b]	location
increasing the $E_{sq/hq}$ difference between XDH and XO				
Lys433	40	152	−112	loop[c]
Glu263	−177	−104	−73	
Asp429	−137	−66	−71	loop[c]
Asp430	−108	−46	−62	loop[c]
Asp360	−236	−190	−46	
Arg426	88	125	−37	loop[c]
Asn71	−14	15	−29	
Glu267	−32	−10	−22	
FeS-II[d]	−151	−129	−22	
Gln144	−14	7	−21	
decreasing the $E_{sq/hq}$ difference between XDH and XO				
Lys422	261	155	106	loop[c]
P (proximal)[e]	14	−81	95	
Lys1228	127	80	47	
Lys271	53	22	31	
Lys343	90	67	23	
Ala338	30	10	20	

b	$E_{sq/hq}$(XDH)	$E_{sq/hq}$(XO)	difference[b]
Lys422	261	155	106
Gln423	−2	−5	3
Ala424	4	−1	5
Ser425	5	1	4
Arg426	88	125	−37
Arg427	21	23	−2
Glu428	−39	−26	−13
Asp429	−137	−66	−71
Asp430	−108	−46	−62
Ile431	9	−6	15
Ala432	10	−2	12
Lys433	40	152	−112
total	152	304	−152

[a]Protein components that increase/decrease the $E_{sq/hq}$ difference by ≥20 mV are listed. For clarity, other residues are omitted from the table. For further information (side chain/backbone contributions), see Table S4 in Supporting Information . [b]$E_{sq/hq}$(XDH) − $E_{sq/hq}$(XO). A negative value here indicates an increased difference between $E_{sq/hq}$ in the two enzymes, while a positive value indicates a decreased difference. [c]The loop region (Gln423−Lys433) close to the flavin ring.[5] [d]The iron−sulfur cluster proximal to the flavin ring. [e]A phosphate titratable site of the FAD diphosphate region proximal to the flavin ring.

redox potentials of the flavin or the iron−sulfur clusters (e.g., refs 39 and 40).

Ribitol Phosphate. The influence of the proximal phosphate region on $E_{sq/hq}$ is calculated to be 14 mV for XDH but −81 mV in XO, a significant difference (Table 3), which seems to cover the entire $E_{sq/hq}$ difference of ∼170 mV between XDH and XO. Note that the proximal phosphate was protonated in XDH but deprotonated in XO. However, if we also consider the influence of Glu263 (−177 mV for XDH and −104 mV for XO, Table 3) and Glu267 (−32 mV and −10 mV), the influence of the [phosphate-Glu263-Glu267] group on $E_{sq/hq}$ is at the same level for XDH and XO, downshifting −194 and −196 mV, respectively. The difference in the phosphate
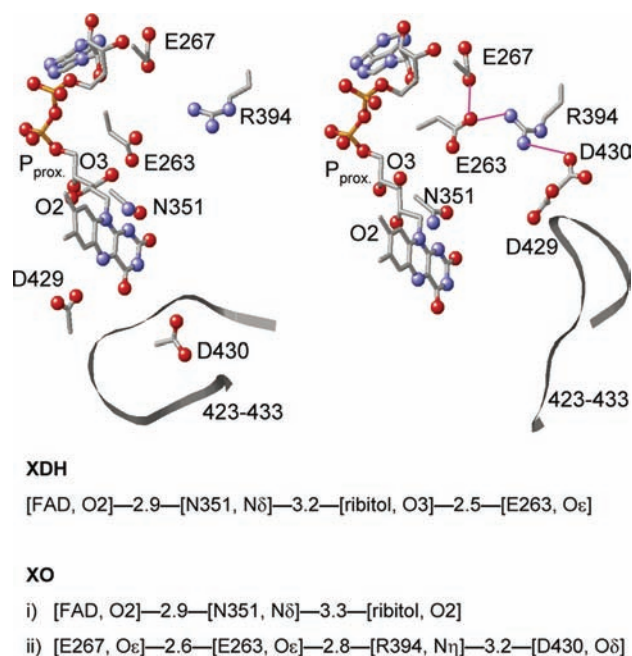

Figure 4. Protein environment of the FAD binding site of XDH (left) and XO (right) and the H-bond network (bottom). N and O atoms are depicted as blue and red balls, respectively. Possible H-bonds, in particular those among Glu263, Glu267, Arg394, and Asp430 are indicated by pink solid lines. $P_{proximal}$ stands for the proximal phosphate atom of the diphosphate region. — — indicates the presence of an H-bond with the numbers giving its length in Ångstrom units.

XDH

[FAD, O2]—2.9—[N351, Nδ]—3.2—[ribitol, O3]—2.5—[E263, Oε]

XO

i) [FAD, O2]—2.9—[N351, Nδ]—3.3—[ribitol, O2]

ii) [E267, Oε]—2.6—[E263, Oε]—2.8—[R394, Nη]—3.2—[D430, Oδ]

contribution to $E_{sq/hq}$ is due to the considerably different Glu263 position and the H-bond network (Figure 4). Glu263 is at H-bond distance from the ribitol O3 atom (2.5 Å) in XDH while the corresponding H bond is absent in XO (4.5 Å from the ribitol O2 atom). Instead, Glu263 forms an H bond with Arg394 (2.8 Å) in XO with the corresponding H bond absent in XDH (4.3 Å). Thus, Glu263 is more tightly involved in the H-bond network around/holding the FAD moiety in XDH whereas it interacts more strongly with the Gln423-Lys433 loop (via Arg394) in XO. In conclusion, the net influence of the [phosphate-Glu263-Glu267] group on $E_{sq/hq}$ is essentially the same in the two proteins.

Calculated Values of $pK_a(N5)$ in XDH and XO. The $pK_a(N5)$ values for FADH•/FAD•− deprotonation were calculated as 12.1 for XDH and 9.6 for XO (Table 4), indicating that the protein environment shifts the $pK_a(N5)$ by 3.5 and 1.0 units, respectively ($pK_a(N5)$ = 8.6 for flavin in aqueous solution).[31] In previous experimental reconstitution studies using 8-hydroxy FAD, it was demonstrated that $pK_a(N5)$ values were upshifted by 3.5 for XDH and 0.1 for XO with respect to their values in aqueous solution.[41] Similar $pK_a(N5)$ shifts were also obtained when the enzyme was reconstituted with other artificial flavins.[42,43] Thus, the measured and calculated $pK_a(N5)$ shifts for the two enzymes compare very well.

Influence of the Protein Dielectric Volume on $pK_a(N5)$. The protein dielectric volumes almost equally upshift the $pK_a(N5)$ values of the native flavin by 3.0 for XDH and 2.6 for XO with respect to the values in aqueous solution (Table 4). The $pK_a(N5)$ upshifts are due to the loss of solvation energy in the flavin binding site with respect to bulk aqueous solution: thus the protein environments destabilize the charged FAD•− form and facilitate formation of the uncharged FADH• state. The similar amount of the $pK_a(N5)$ upshifts calculated in both XDH

Table 4. $E_{ox/sq}$ and pK_a(N5) in mV and pK_a Units, Respectively[a]

		XDH		XO	
		E_m	pK_a	E_m	pK_a
$E_{ox/sq}$ ($= E_m$(FAD/FAD⁻)) $+ RT/F$ ln10 log(1 + $10^{-(pH-pKa(N5))}$)[d]	experimental	−270[b]		−332[c]	
	calculated	−296		−322	
	uncharged protein[e]	−298		−301	
	reference (water)[f]	−238		−238	
$E_{ox/sq}$ shift (from water to protein)	Total	−14		−40	
	ΔE_m(charge)[h]	1		−21	
	ΔE_m(dielectric volume)[i]	−16		−19	
a) E_m(FAD/FAD⁻)	experimental	n.d.[g]		n.d.[g]	
	calculated	−550		−429	
	uncharged protein[e]	−520		−502	
	reference (water)[f]	−333		−333	
E_m shift (from water to protein)	Total	−217		−96	
	ΔE_m(charge)[h]	−30		73	
	ΔE_m (dielectric volume)[i]	−187		−169	
b) pK_a(N5) for FADH•/FAD•⁻	experimental		n.d.		n.d.
	calculated		12.1		9.6
	uncharged protein[e]		11.6		11.2
	reference (water)[f]		8.6		8.6
pK_a shift (from water to protein)	Total		3.5		1.0
	ΔpK_a (charge)[h]		0.5		−1.6
	ΔpK_a (dielectric volume)[i]		3.0		2.6
b′) corresponding E_m term i.e., RT/F ln10 log(1 + $10^{-(pH-pKa(N5))}$)	experimental	n.d.[g]		n.d.[g]	
	calculated	254		107	
	uncharged protein[e]	222		201	
	reference (water)[f]	51		51	
E_m shift (from water to protein)	Total	203		56	
	ΔE_m (charge)[h]	31		−94	
	ΔE_m (dielectric volume)[i]	171		150	

[a]$E_{ox/sq}$ are discussed in "Calculated values of $E_{ox/sq}$ in XDH and XO". [b]At pH 7.5.[3] [c]At pH 7.7.[4] [d]See ref.[12] [e]Prepared by setting atomic charges of all atoms in the protein to zero. [f]See ref.[31] [g]Not determined. [h]Influence of atomic charge of all atoms in the protein. [i]Influence of uncharged protein dielectric volume (i.e., the space covered by the merged van der Waals volumes of protein atoms).

and XO imply that the protein dielectric volume (or "protein hydrophobicity" in terms of the loss of solvation energy) does not differ considerably. (Note: In the protein inner core, the major contributor toward destabilizing charged groups is, in many cases, loss of solvation energy, rather than repulsive interactions.[38])

Influence of the Protein Atomic Charge on pK_a(N5). The pK_a(N5) difference between XDH and XO is dominated by the influence of the protein atomic charges. The atomic charge influence on pK_a(N5) is −1.6 in XO whereas 0.5 in XDH (Table 4). As a consequence, the anionic FAD•⁻ form can be more effectively stabilized in XO than in XDH (although the native flavin is in the neutral charge FADH• form in both enzymes due to their high pK_a(N5) values of >8).

In agreement with the calculated lower pK_a(N5) value in XO than XDH, it is experimentally observed that artificial flavins reconstitute with apoprotein in their uncharged, neutral forms for XDH but in their anionic forms for XO.[41−44] Hence the anionic FAD•⁻ state in XO is more effectively stabilized by charged residues than in XDH. For instance, the positively charged Lys433 stabilizes the FAD•⁻ state more effectively in XO than XDH, contributing to the increase in the pK_a(N5) difference for the two enzymes (Table S6 in the Supporting Information). Many residues that contribute to the difference of the pK_a(N5) values between XDH and XO are located in the 423−433 region, namely Asp430, Asp429, and Arg426. Again, as seen in the analysis of the $E_{sq/hq}$ difference, the loop region is likely the most crucial part that characterizes the flavin electrostatic environment for XDH and XO.

In previous studies, the apparently different pK_a(N5) values were considered to be due to the presence/absence of a strong negative charge in XDH/XO (reviewed in ref 2). However, the present computation suggests that the difference in the flavin electrostatics can not be attributed to a specific single residue but is well understood as caused by the sum of contributions from a number of charged residues, including the proximal phosphate.

Calculated Values of $E_{ox/sq}$ in XDH and XO. By calculating E_m(FAD/FAD•⁻) and pK_a(N5) and by using eq 1, the $E_{ox/sq}$ values (i.e., E_m(FAD/FADH•)) of −296 mV for XDH and −322 mV for XO were obtained (Table 4). These values are in good agreement with the experimentally measured $E_{ox/sq}$ values of −270 mV[3] and −332 mV[4] for XDH and XO, respectively. In contrast to the significant $E_{sq/hq}$ difference of ∼170 mV for XDH and XO, the $E_{ox/sq}$ values are essentially at the same level for XDH and XO. A similar tendency, where $E_{ox/sq}$ values are less correlated with protein electrostatic environment (e.g., mutation of charged residues), has been observed before in other proteins containing flavin cofactors.[45,46]

The reason for the resulting similar $E_{ox/sq}$ values of the two enzymes irrespective of the different protein environment (e.g., see $E_{sq/hq}$ values) can be understood as follows:

$$\text{FAD} \rightarrow \text{FAD}^{\bullet-} \rightarrow \text{FADH}^{\bullet} \qquad (2)$$

The FAD/FADH• equilibrium proceeds via the FAD•⁻ state as presented in eq 2. In the initial FAD/FAD•⁻ redox process, XO stabilizes the reduced FAD•⁻ state due to the more positively charged flavin binding site, leading to an increase in the E_m(FAD/FAD•⁻) term in eq 1. This also holds true for the next FAD•⁻/FADH• protonation process: the positively charged environment of the flavin binding site in XO (relative to XDH) energetically favors the deprotonated FAD•⁻ state with respect to the uncharged FADH• state; thus, the pK_a(N5) value in XO is lower than in XDH (Table 4). As a consequence, the RT/F ln10 log(1 + $10^{-pH}/10^{-pKa(N5)}$) term in eq 1 decreases. Thus, the increased E_m(FAD/FAD•⁻) term is compensated for by the decreased RT/F ln10 log(1 + $10^{-pH}/10^{-pKa(N5)}$) term.

In contrast, the charge neutral environment in XDH does not energetically favor the charged FAD•⁻ state in comparison with XO, resulting in a decrease in the E_m(FAD/FAD•⁻) term and an increase in the RT/F ln10 log(1 + $10^{-pH}/10^{-pKa(N5)}$) term. Here, the decreased E_m(FAD/FAD•⁻) term is compensated for by the increased RT/F ln10 log(1 + $10^{-pH}/10^{-pKa(N5)}$) term (Table 4).

Although the protein environments have almost opposite influences on the shift of the flavin energetics for the two enzymes, they result in almost equal $E_{ox/sq}$ values for the two enzymes, since changes in the E_m(FAD/FAD•⁻) and RT/F
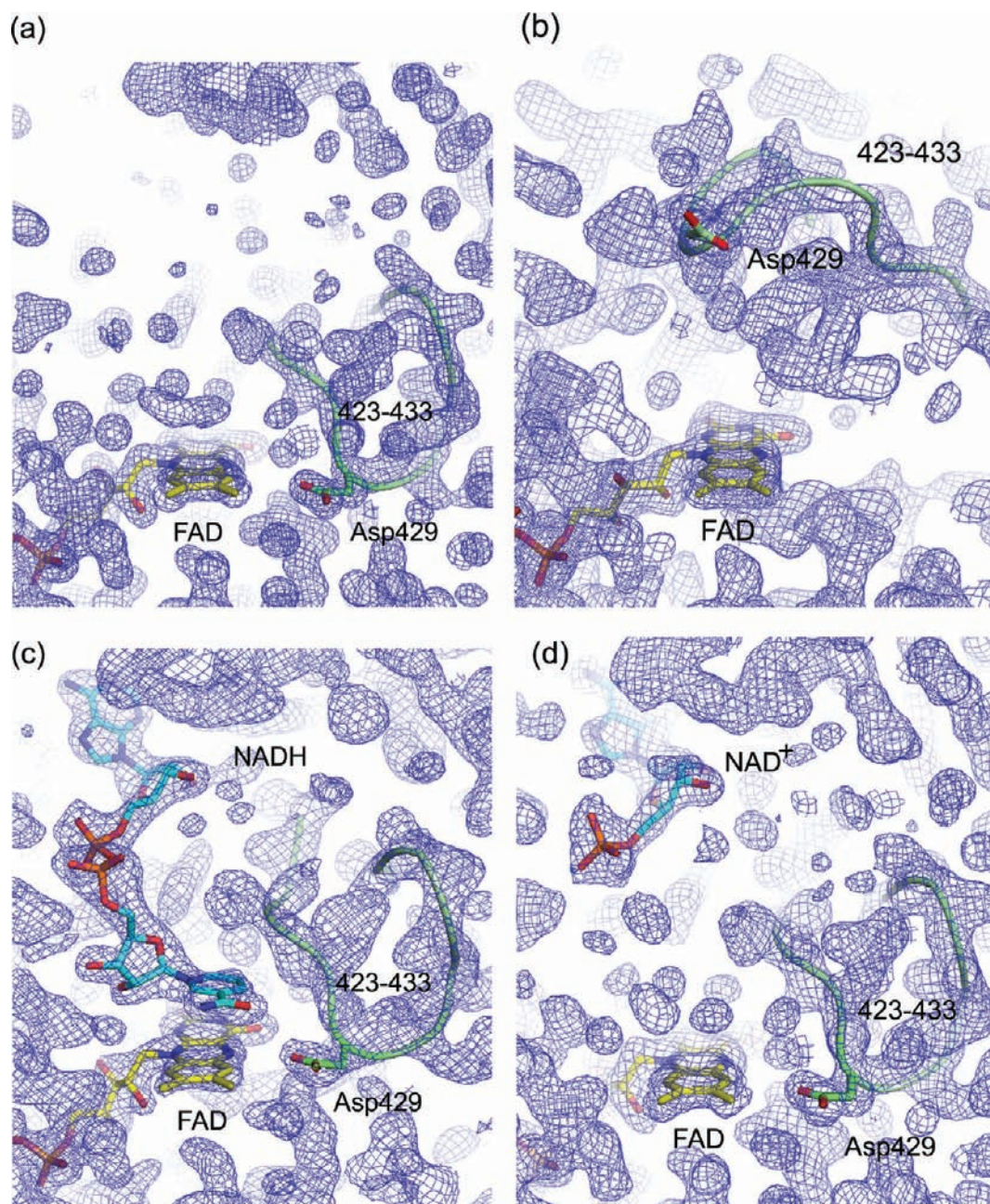
Figure 5. Electron density maps of the FAD and NAD(H) binding sites in (a) ligand-free XDH, (b) ligand-free XO, (c) the XDH-NADH complex, and (d) the XDH-NAD$^+$ complex. For clarity, only the FAD, NAD(H), and Asp429 are shown in atom representation. The backbone trace of the 423−433 loop is indicated by a green thread. Although the loop seems to swing away from the flavin ring in XO, it does interfere with dinucleotide access in its new location.

ln10 log$(1 + 10^{-pH}/10^{-pKa(N5)})$ terms practically cancel out each other.

2. NAD+/NADH Binding to XDH. *Crystal Structures of the NAD$^+$ and NADH Complexes of Bovine XDH.* The 1.9 and 2.2 Å resolution crystal structures of the NAD$^+$ and NADH complexes of bovine XDH, respectively, confirm the overall fold of the dimeric proteins, the location of the cofactors and the mobile stretches of the polypeptide chains.[5] In both structures, the adenine half of the NAD(H) molecules binds at the surface of the protein surrounded by residues Glu263, Ser356, Tyr393, Arg394, and Pro501. The remainder of the dinucleotide extends into an open cavity leading toward the flavin ring. While the electron density for the oxidized dinucleotide only extends to

the first half of the pyrophosphate group, the full molecule of NADH is clearly visible and well-defined in the electron density map (Figure 5a and b). The nicotinamide ring lies parallel to the flavin ring undergoing a π-stacking interaction as found in many other structurally characterized NAD-flavin complexes.[47−52]

The two crystal structures complexed with NAD$^+$ and NADH did not significantly differ in the position/orientation of the flavin ring, the adenine half of the NAD(H), and the loop 423−433 (backbone and side chains).

$E_{sq/hq}$ Upshift Due to NAD$^+$ Binding. The calculated $E_{sq/hq}$ value for XDH complexed to NAD$^+$ was −226 mV, resulting in a ~180 mV upshift relative to the calculated $E_{sq/hq}$ value of −407 mV for ligand-free XDH (Table 2, Figure 3b). Since the

1006

dx.doi.org/10.1021/ja207173p | *J. Am. Chem. Soc.* 2012, 134, 999−1009

E_m value for the electron donor FeS-II is −235 mV,[3] ET from FeS-II to sq/hq would be energetically uphill (+175 meV, dotted arrow in Figure 6) before NAD$^+$ binding. The ligand
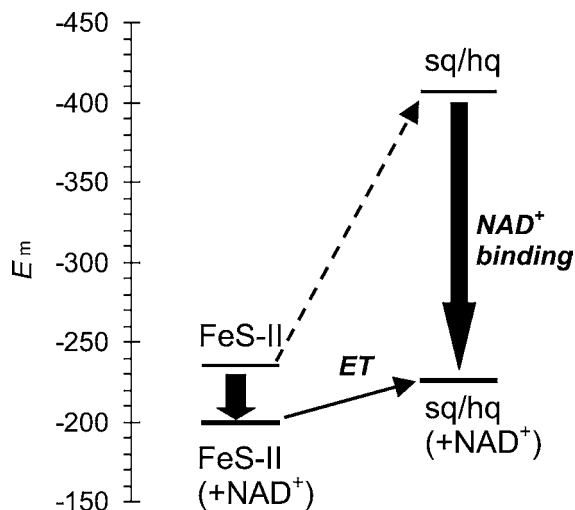

Figure 6. Shift in the redox potential levels and energetics for ET from FeS-II to flavin (sq/hq) in response to NAD$^+$ binding. The solid black arrows indicate the redox potential shifts due to the NAD$^+$ binding.

binding also induces an upshift in E_m(FeS-II) but this one is considerably smaller (+35 mV). Thus, the ET was transformed into an almost isoenergetic process (+20 meV), facilitating the forward ET dramatically (Figure 6); this result confirms a scheme previously proposed for ET from FeS-II to sq/hq.[7,8]

Interestingly, the change in $E_{sq/hq}$ of ~180 mV is about the same as the $E_{sq/hq}$ difference between XDH ($E_{sq/hq}$ = −410 mV[3]) and XO (−234 mV[4]). In the present study, we found that the 423−433 loop, which changes its conformation drastically when XDH is transformed into XO (Figure 2), is the major cause for the $E_{sq/hq}$ difference of ~140 mV between XDH and XO (Table 3b). In contrast, we did not observe significant structural changes for this loop upon NAD(H) binding, denying the possibility that the same loop might be responsible for both E_m differentials.

Contribution of the Atomic Charge of NAD$^+$ to the $E_{sq/hq}$ Shift. From a comparison between the calculated $E_{sq/hq}$ value for the protein and the calculated $E_{sq/hq}$ value for the "uncharged" protein (i.e., the protein dielectric volume where all the atomic partial charges in the protein except for the flavin part (flavin = isoalloxazine ring and ribitol region) are set to zero), the influence of the protein atomic charge on $E_{sq/hq}$ can be obtained. In the present study, the $E_{sq/hq}$ values are shifted down by 64 mV for ligand-free XDH but shifted up by 180 mV for XDH with NAD$^+$ bound due to the atomic partial charges on the entire protein (Table 2). Since the two states, ligand-free XDH and the NAD$^+$-complex of the enzyme differ only in the absence or presence of the NAD$^+$ molecule, the resulting $E_{sq/hq}$ upshift of 240 mV should be caused by the positive charge on the NAD$^+$ ring region (note, the net charge of the entire NAD$^+$ molecule is not +1 due to the diphosphate region).

However, further analysis revealed that the total effect of the NAD$^+$-ring charge on $E_{sq/hq}$ is 358 mV (Table 5), which is much larger than the observed $E_{sq/hq}$ difference of 240 mV. Thus, there must exist other contributions that partially compensate for the $E_{sq/hq}$ effect of NAD$^+$ binding. Asp429 has been identified as the factor that predominantly compensates for the influence of

Table 5. Protein Components Increasing the $E_{sq/hq}$ Value and Compensating for the $E_{sq/hq}$ Up-shift in Response to NAD$^+$ Binding in mV[a]

	$E_{sq/hq}$(XDH)	$E_{sq/hq}$(XDH with NAD$^+$)	difference[b]
components increasing the $E_{sq/hq}$ value			
NAD$^+$		358	358
Lys422	261	323	62
P (NAD$^+$, proximal)[c]		36	36
Arg394	60	90	30
Lys343	90	114	24
compensating for the $E_{sq/hq}$ upshift			
Asp429	−137	−253	−116
Glu263	−177	−257	−80
Asp360	−236	−312	−76
FeS-II[d]	−151	−183	−32
Asp430	−108	−134	−26
P (FAD, distal)[e]	−75	−97	−22

[a]Protein components that increase/decrease the $E_{sq/hq}$ difference by ≥20 mV are listed. For clarity, other residues are omitted from the table. For further information (side chain/backbone contributions), see Table S5 in Supporting Information. [b]$E_{sq/hq}$(XDH with NAD$^+$) − $E_{sq/hq}$(XDH). A positive value here indicates an increased difference between $E_{sq/hq}$ in the two enzymes, while an negative value indicates a decreased difference. [c]A phosphate titratable site of the NAD$^+$ diphosphate region proximal to the nicotinamide ring. [d]The iron−sulfur cluster proximal to the flavin ring. [e]Phosphate titratable site of the FAD diphosphate region distal to the flavin ring.

the positive NAD$^+$-ring charge on $E_{sq/hq}$. In response to NAD$^+$ binding, it alters its protonation state (Figure 3b), becoming less protonated after complex formation (0.4 H$^+$ for the FADH$^-$ state) than in the ligand-free enzyme (0.8 H$^+$ for the FADH$^-$ state).

Since Asp429 is located only ~3 Å away from the flavin ring, its ionization state impacts $E_{sq/hq}$ significantly. In particular, the carboxyl O atom of Asp429 is not only close to the flavin (O$_{Asp429}$−C6$_{flavin}$ = 3.2 Å) but also to the nicotinamide region (O$_{Asp429}$−O7$_{NAD^+}$ = 3.6 Å). Thus, the more deprotonated Asp429 induced by the binding of the positively charged NAD$^+$ ring destabilizes the anionic FADH$^-$ state, thus downshifting $E_{sq/hq}$. In contrast to the strong coupling with the flavin redox state observed in ligand-free XDH and the NAD$^+$-complex of XDH, Asp429 did not change its protonation state in response to the flavin redox state in XO (Figure 3a). The absence of such a coupling between Asp429 protonation state and flavin redox state in XO implies that Asp429 is not required in XO function, probably reflecting its inability to utilize NAD$^+$ as a substrate due to steric hindrance (Figure 5b).

Interestingly, Glu59 in *Clostridium beijerinckii* flavodoxin and Asp62 in *Desulfovibrio vulgaris* flavodoxin are located at corresponding positions: the two acidic residues also change their protonation states in response to the redox state of their flavin.[12,13] The presence of acidic residues that change their protonation states near the flavin might be a common feature, which might be useful to keep $E_{sq/hq}$ values constant by buffering changes in any external electrostatic influence.

Contribution of NAD$^+$ volume to the $E_{sq/hq}$ shift. The protein dielectric volume (i.e., the space obtained by merging the volumes of the van der Waals spheres of all protein atoms) is a main contributor to so-called "protein hydrophobicity" affecting the flavin cofactor: it prevents access of water molecules to the flavin, and thus decreases the availability of solvation

energy. In particular, the loss of solvation energy[38] destabilizes the FADH⁻ state significantly, leading to the decrease in $E_{sq/hq}$.

By comparing the $E_{sq/hq}$ value of flavin in water (−172 mV) with the $E_{sq/hq}$ value of the "uncharged" (i.e., where all the atomic partial charges in the protein except for the flavin part (flavin = isoalloxazine ring and ribitol region) are set to zero) protein (−343 mV for ligand-free XDH and −406 mV for the NAD⁺-complex of XDH), we determined that the protein dielectric volume shifts the $E_{sq/hq}$ value by −171 mV for the ligand-free enzyme and by −234 mV for the NAD⁺-complex (Table 2). The larger $E_{sq/hq}$ downshift indicates that the flavin molecule is less exposed to the bulk solvent in the NAD⁺-complex of XDH (Figure 7) and that XDH with NAD⁺ bound cannot stabilize the
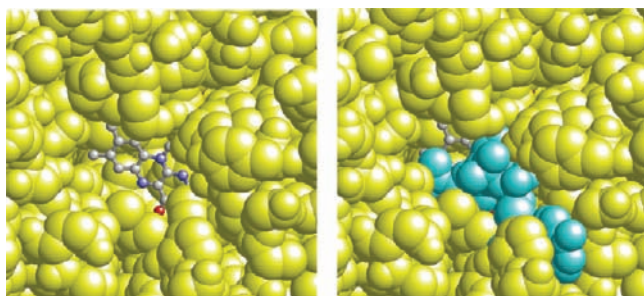
Figure 7. Representation of the FAD site of XDH. In the left-hand figure, the NADH molecule has been removed to indicate the water-accessible area of the flavin ring. In the right-hand figure, the same view is given but with the NADH molecule included to show how well the NADH molecule covers the flavin ring. The FAD atoms are depicted as ball-and-stick while the NADH molecule (cyan) and the protein atoms (yellow) are depicted as space-filling models.

anionic FADH⁻ state effectively. As a result, the NAD⁺ volume that now covers the water accessible surface of the flavin (Figure 7) contributes to the $E_{sq/hq}$ downshift of 63 mV, counteracting the $E_{sq/hq}$ upshift caused by the positive charge of NAD⁺ ring.

CONCLUSIONS

The new 1.65 and 2.3 Å resolution crystal structures for XDH and XO, respectively, confirmed the side chain orientation in details. In particular the two crystal structures revealed the difference in the protein environment of the FAD binding site and the H-bond network for XDH and XO (Figure 4). This enabled us to precisely determine the protonation states of the titratable residues including those in the 423−433 loop, reproduce $E_{sq/hq}$ values, and thus pinpoint the factors that differentiate $E_{sq/hq}$ values between the two enzymes. The highly charged loop near the flavin-binding site is the main factor that differentiates the $E_{sq/hq}$ between XDH and XO. The difference in the $E_{sq/hq}$ between XDH and XO is 150 mV when calculated over the region of residues 422−433 (Table 3b). The influence of the protein dielectric volume (that prevents access to the flavin from water) on $E_{sq/hq}$ is equal in XDH and XO.

The crystal structures of the NAD(H) complexes of XDH revealed that, given the proper oxidation states, the nicotinamide rings of the dinucleotides locate at van der Waals distance to the flavin ring. A conformational change in the 423−433 loop region was not observed in response to NAD(H) binding. Instead, NAD⁺ binding to XDH is the switch that facilitates the forward ET from FeS-II to flavin, by upshifting $E_{sq/hq}$ by ~180 mV to yield an isoenergetic ET. The influence of the positive NAD⁺-ring charge on $E_{sq/hq}$ (upshifting by 360 mV) is

partly compensated by (i) deprotonation of Asp429 (down-shifting $E_{sq/hq}$ by 120 mV, Table 5) and (ii) the van der Waals volume of the NAD⁺ molecule. In XDH, the protonation state of Asp429 changes significantly in response to the flavin redox change during titration for $E_{sq/hq}$ but not in XO (Figure 3). This is of no consequence in the latter because of XO's inability to bind NAD⁺ due to steric interference by the 423−433 loop.

Whether the 423−433 loop locates away from the flavin ring but still interfering with NAD(H) binding (i.e., in XO) or approaches the flavin part of FAD and thereby contributing to the binding site of NADH (i.e., in XDH) discriminates the $E_{sq/hq}$ by ~170 mV. The former is advantageous for the forward ET from FeS-II to flavin but cannot host NAD⁺/NADH as the successive electron acceptor for the flavin due to the obstructed binding pocket. On the other hand, the XDH form is apparently of disadvantage for the ET from FeS-II due to the quite low $E_{sq/hq}$, but it can host NAD⁺/NADH in the neighborhood of the flavin. Employing the external NAD⁺ as an electron acceptor of the flavin upshifts $E_{sq/hq}$ significantly by ~180 mV, simultaneously reducing the energetic barrier for the successive ET. The similar $E_{sq/eq}$ differences of ~180 mV for XDH/XO and XDH/XDH-NAD⁺ imply the energetic compensation for $E_{sq/hq}$ of the different conformations of the 423−433 loops by NAD⁺ binding.

ASSOCIATED CONTENT

ⓢ Supporting Information

Complete ref 27, atomic charges, discussion about dielectric constant, and residues/groups that shift E_m or pK_a of flavin. This material is available free of charge via the Internet at http://pubs.acs.org.

AUTHOR INFORMATION

Corresponding Author

hiro@cp.kyoto-u.ac.jp

ACKNOWLEDGMENTS

■ REFERENCES

(1) Saito, T.; Nishino, T. *J. Biol. Chem.* **1989**, *264*, 10015−10022.

(2) Nishino, T.; Okamoto, K.; Eger, B. T.; Pai, E. F.; Nishino, T. *FEBS J.* **2008**, *275*, 3278−3289.

(3) Hunt, J.; Massey, V.; Dunham, W. R.; Sands, R. H. *J. Biol. Chem.* **1993**, *268*, 18685−18691.

(4) Barber, M. J.; Siegel, L. M. *Biochemistry* **1982**, *21*, 1638−1647.

(5) Enroth, C.; Eger, B. T.; Okamoto, K.; Nishino, T.; Pai, E. F. *Proc. Natl. Acad. Sci. U.S.A.* **2000**, *97*, 10723−10728.

(6) Rabenstein, B.; Ullmann, G. M.; Knapp, E.-W. *Biochemistry* **2000**, *39*, 10487−10496.

(7) Nishino, T.; Okamoto, K. *J. Inorg. Biochem.* **2000**, *82*, 43−49.

(8) Nishino, T.; Nishino, T. *J. Biol. Chem.* **1989**, *264*, 5468−5473.

(9) Ishikita, H.; Knapp, E.-W. *FEBS Lett.* **2005**, *579*, 3190−3194.

(10) Ishikita, H.; Knapp, E.-W. *Biochemistry* **2005**, *44*, 14772−14783.

(11) Hille, R. *Chem. Rev.* **1996**, *96*, 2757−2816.

(12) Ishikita, H. *J. Biol. Chem.* **2007**, *282*, 25240−25246.

(13) Ishikita, H. *Biochemistry* **2008**, *47*, 4394−4402.

(14) Ishikita, H. *J. Biol. Chem.* **2008**, *283*, 30618−30623.

(15) Eger, B. T.; Okamoto, K.; Enroth, C.; Sato, M.; Nishino, T.; Pai, E. F. *Acta Crystallogr., D: Biol. Crystallogr.* **2000**, *56*, 1656−1658.

(16) Otwinowski, Z.; Minor, W. *Methods Enzymol.* **1997**, *276*, 307−326.

(17) Brunger, A. T.; Adams, P. D.; Clore, G. M.; DeLano, W. L.; Gros, P.; Grosse-Kunstleve, R. W.; Jiang, J. S.; Kuszewski, J.; Nilges, M.; Pannu, N. S.; Read, R. J.; Rice, L. M.; Simonson, T.; Warren, G. L. *Acta Crystallogr., D: Biol. Crystallogr.* **1998**, *54*, 905−921.

(18) Kirschbaum, M. U. F.; Farquhar, G. D. *Aust. J. Plant Physiol.* **1984**, *11*, 519−538.

(19) Vagin, A.; Teplyakov, A. *J. Appl. Crystallogr.* **1997**, *30*, 1022−1025.

(20) Collaborative Computational Project. *Acta Crystallogr., D: Biol. Crystallogr* **1994**, *50*, 760−763.

(21) Jones, T. A. *J. Appl. Crystallogr.* **1978**, *11*, 268−272.

(22) Emsley, P.; Lohkamp, B.; Scott, W. G.; Cowtan, K. *Acta Crystallogr., D: Biol. Crystallogr* **2010**, *66*, 486−501.

(23) Brooks, B. R.; Bruccoleri, R. E.; Olafson, B. D.; States, D. J.; Swaminathan, S.; Karplus, M. *J. Comput. Chem.* **1983**, *4*, 187−217.

(24) Mouesca, J.; Chen, J. L.; Noodleeman, L.; Bashford, D.; Case, D. A. *J. Am. Chem. Soc.* **1994**, *116*, 11898−11914.

(25) Ishikita, H.; Knapp, E.-W. *J. Biol. Chem.* **2003**, *278*, 52002−52011.

(26) Bayly, C. I.; Cieplak, P.; Cornell, W. D.; Kollman, P. A. *J. Phys. Chem.* **1993**, *97*, 10269−10280.

(27) Frisch, M. J.,et al. *Gaussian 03*; Gaussian, Inc.: Wallingford, CT, 2004.

(28) Bashford, D.; Karplus, M. *Biochemistry* **1990**, *29*, 10219−10225.

(29) Rabenstein, B.; Knapp, E. W. *Biophys. J.* **2001**, *80*, 1141−1150.

(30) Ishikita, H.; Knapp, E.-W. *J. Biol. Chem.* **2005**, *280*, 12446−12450.

(31) Draper, R. D.; Ingraham, L. L. *Arch. Biochem. Biophys.* **1968**, *125*, 802−808.

(32) Kumler, W. D.; Eiler, J. J. *J. Am. Chem. Soc.* **1943**, *65*, 2355−2361.

(33) McElroy, W. D.; Glass, B. *Phosphorus Metabolism*, Volume *I*; Johns Hopkins University Press: Baltimore, 1951.

(34) Swallow, A. J. In *Function of Quinones in Energy Conserving Systems*; Trumpower, B. L., Ed.; Academic Press: New York, 1982; pp 59−72.

(35) Porras, A. G.; Palmer, G. *J. Biol. Chem.* **1982**, *257*, 11617−11626.

(36) Tommos, C.; Skalicky, J. J.; Pilloud, D. L.; Wand, A. J.; Dutton, P. L. *Biochemistry* **1999**, *38*, 9495−9507.

(37) Ludwig, M. L.; Schopfer, L. M.; Metzger, A. L.; Pattridge, K. A.; Massey, V. *Biochemistry* **1990**, *29*, 10364−10375.

(38) Kato, M.; Pisliakov, A. V.; Warshel, A. *Proteins* **2006**, *64*, 829−844.

(39) Cammack, R.; Barber, M. J.; Bray, R. C. *Biochem. J.* **1976**, *157*, 469−478.

(40) Nishino, T.; Amaya, Y.; Kawamoto, S.; Kashima, Y.; Okamoto, K.; Nishino, T. *J. Biochem.* **2002**, *132*, 597−606.

(41) Massey, V.; Schopfer, L. M.; Nishino, T. *J. Biol. Chem.* **1989**, *264*, 10567−10573.

(42) Hunt, J.; Massey, V. *J. Biol. Chem.* **1992**, *267*, 21479−21485.

(43) Saito, T.; Nishino, T.; Massey, V. *J. Biol. Chem.* **1989**, *264*, 15930−15935.

(44) Ghisla, S.; Massey, V. *Biochem. J.* **1986**, *239*, 1−12.

(45) Zhou, Z.; Swenson, R. P. *Biochemistry* **1995**, *34*, 3183−3192.

(46) McCarthy, A. A.; Walsh, M. A.; Verma, C. S.; O'Connell, D. P.; Reinhold, M.; Yalloway, G. N.; d'Arcy, D.; Higgins, T. M.; Voordouw, G.; Mayhew, S. G. *Biochemistry* **2002**, *41*, 10950−10962.

(47) Pai, E. F.; Karplus, P. A.; Schulz, G. E. *Biochemistry* **1988**, *27*, 4465−4474.

(48) Stehle, T.; Claiborne, A.; Schulz, G. E. *Eur. J. Biochem.* **1993**, *211*, 221−226.

(49) Senda, T.; Yamada, T.; Sakurai, N.; Kubota, M.; Nishizaki, T.; Masai, E.; Fukuda, M.; Mitsuidagger, Y. *J. Mol. Biol.* **2000**, *304*, 397−410.

(50) Chiu, H. J.; Johnson, E.; Schroder, I.; Rees, D. C. *Structure* **2001**, *9*, 311−319.

(51) van den Heuvel, R. H.; Westphal, A. H.; Heck, A. J.; Walsh, M. A.; Rovida, S.; van Berkel, W. J.; Mattevi, A. *J. Biol. Chem.* **2004**, *279*, 12860−12867.

(52) Pudney, C. R.; Hay, S.; Levy, C.; Pang, J.; Sutcliffe, M. J.; Leys, D.; Scrutton, N. S. *J. Am. Chem. Soc.* **2009**, *131*, 17072−17073.

(53) Ullmann, G. M.; Knapp, E.-W. *Eur. Biophys. J.* **1999**, *28*, 533−551.